J. CHEM. SOC. FARADAY TRANS., 1994, 90(16), 2375–2380

Monte Carlo Simulations of a Single Poly(oxyethylene) $C_{12}E_2$ Chain Headgroup fixed on a Bilayer Surface in Water

Y. C. Kong, D. Nicholson and N. G. Parsonage
Department of Chemistry, Imperial College of Science, Technology and Medicine, London, UK SW7 2AY
L. Thompson
Unilever Research, Port Sunlight Laboratory, Quarry Road East, Bebbington, Wirral, Merseyside, UK L63 3JW

Monte Carlo simulations of a single poly(oxyethylene) $C_{12}E_2$ surfactant chain headgroup attached to the hydrophobic wall of a bilayer have been performed at various temperatures. The structure of the water around the chain was examined by collecting radial distribution functions and densities for different regions in the plane of the bilayer surface. There is a strong tendency for water to form H-bonded 'bridges' between adjacent oxygen atoms on the same chain and to favour *gauche* conformations for the O—C—C—O torsional angles, the effect being weaker the higher the temperature. Water molecules have a weaker tendency to form bridges between non-adjacent oxygen atoms within the chain. The observed *gauche/trans* ratio increase and stronger chain adsorption which are found with increasing temperature were explained by relatively weaker water–chain interactions and a more dominant chain–wall interaction at higher temperatures.

The stability of surfactant or lipid bilayers is important in understanding colloid science and biology. Classical colloid theory (DLVO) does not provide an adequate explanation. In the DLVO theory long-range van der Waals attractions are balanced by shorter-range electrostatic double-layer forces. The double-layer repulsive forces would be much weaker for non-ionic or zwitterionic headgroups and the DLVO theory would suggest that the bilayer would collapse. However, bilayers are found to be stable and it is necessary to invoke a new force, termed the 'hydration force', to explain this stability.

Tiddy and co-workers[1,2] have measured the equilibrium vapour pressure of water above aqueous lamellar (L_α) phases of poly(oxyethylene) surfactants $C_nH_{2n+1}(OCH_2CH_2)_mOH$ for various bilayer separations. The interbilayer repulsive pressure as a function of separation was calculated from the vapour pressure. Claesson *et al.*[3] have measured directly the forces between hydrophobic mica surfaces coated with poly(oxyethylene) surfactants and submerged in water.

Although both vapour pressure and mica experiments indicated the existence of the hydration force, the temperature dependence of the observed force was different. In the vapour pressure experiment the hydration force became more repulsive with increased temperature, whereas in the mica experiment repulsion decreased with temperature and the force became attractive at some separations. This contradiction was explained by invoking thermal undulation of the adjacent bilayers which cause the point of closest contact at any given time to be much nearer than the time-averaged separation.[4] Repulsion due to undulation was attributed to steric overlaps between headgroups at the closest point of contact. Such forces increase with temperature and are not possible for surfactants adsorbed onto a rigid mica surface.

The presence of the solvent is an essential factor. Simulations[5] and theoretical[6,7] models which have excluded discrete solvent molecules have failed to predict a repulsion. Hence, it appears to be the ability of the solvent to hydrogen bond,[8] rather than the existence of a dipole, which is important in the stabilization of lamellar phases in poly(oxyethylene) surfactant–solvent systems.

There are two likely sources of the hydration repulsion: (1) The partial charges on the ethoxy groups which influence the structure of water in their vicinity and (2) the structural effects due to the possibility of multiple chain conformations.

Marčelja and co-workers[9–12] have highlighted the likely importance of the first of these two factors, claiming that perturbation of surface water structure is propagated into the solvent. Cracknell and co-workers[13,14] have simulated the effect of surface partial charges on the structure of the water using the model illustrated in Fig. 1. Their computer simulation showed that local water structure was modified by the surface charges, but this did not result in a stable bilayer.

However, Cracknell and co-workers[13,15] also showed, using an elementary statistical mechanical model that the repulsion between bilayers can be predicted from consideration of the entropy associated with a multiplicity of binding sites in an ethoxy chain.

It is the aim of this work to introduce flexible poly(oxyethylene) chains into the simulation model previously investigated by Cracknell. As a first step a single fixed poly(oxyethylene) $C_nH_{2n+1}(OCH_2CH_2)_2OH$ attached to a hydrocarbon bilayer has been simulated at various temperatures. Statistical sampling was carried out to investigate the perturbation of the interfacial water and the relative numbers of *gauche* and *trans* chain conformations. The SPC water potential was used here because it gives a better relative permittivity and more accurate water distribution functions than the TIPS2 used in earlier work.

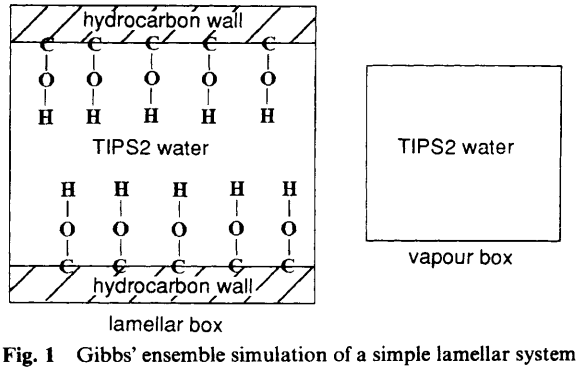

Fig. 1 Gibbs' ensemble simulation of a simple lamellar system

Method

A single attached $C_nH_{2n+1}(OCH_2CH_2)_2OH$ surfactant molecule was studied using Monte Carlo simulation in the canonical ensemble (NVT) illustrated in Fig. 2. The water was modelled as a Lennard-Jones centre with three point charges using the SPC[16] model. The chain CH_2 groups on the chain atoms were modelled as united atoms and the oxygens and the terminating hydrogen as discrete atoms. A partial charge was placed on these atoms, taken from the OPLS[17] set. The oxygen was assigned a negative charge and counter charges were placed on the adjacent CH_2 pseudo-atom and the terminating hydrogen. Dispersion interactions were represented by 12-6 potentials with the parameters given in Table 1. Mixed interaction parameters were calculated from the Lorentz rules. The dimensions and numbering convention for the chain are shown in Fig. 3. The bond torsional interaction was modelled using a Fourier expansion:[17]

$$u = \frac{V_1}{2}(1 + \cos\phi) + \frac{V_2}{2}(1 - \cos 2\phi) + \frac{V_3}{2}(1 + \cos 3\phi) + \cdots \quad (1)$$

$$u = c_0 + c_1\cos\phi + c_2\cos^2\phi + c_3\cos^3\phi + \cdots \quad (2)$$

Where the V_i and c_i parameters are related by $c_0 = (V_1 + 2V_2 + V_3)/2$, $c_1 = (V_1 - 3V_3)/2$, $c_2 = -V_2$ and $c_3 = 2V_3$. The OPLS[17,18] chain parameters were used, and the fourth- and higher-order torsional terms were ignored. The values of the Fourier parameters used are given in Table 2.

The hydrocarbon walls were modelled as an infinite number of layers of smeared out CH_2 united atoms (Fig. 4) with a number density/Å^{-3} based on the properties of experimental packed hydrocarbon chains. The Lennard-Jones wall–water/chain potential integrated over an infinite number of layers is:[13]

$$\frac{4\pi\varepsilon\sigma^{12}}{5A_{ch}}\left[\frac{1}{z^{10}} + \frac{1}{9d(z+0.72d)^9}\right] - \frac{2\pi\varepsilon\sigma^6}{A_{ch}}\left[\frac{1}{z^4} + \frac{1}{3d(z+0.60d)^3}\right] \quad (3)$$

Where z is the distance, d is the separation of the CH_2 layers, A_{ch} the cross-sectional area of a chain. The ε and σ constants are the Lennard-Jones parameters for the CH_2 united atoms. Table 3 lists the values used in the simulation.

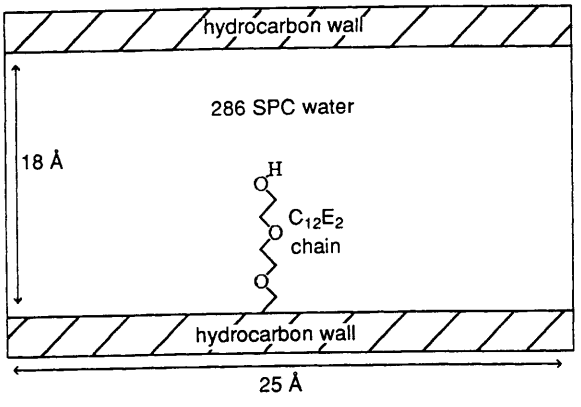

Fig. 2 Single $C_{12}E_2$ chain fixed to a bilayer

Table 1 OPLS Lennard-Jones parameters and point charges for the $C_{12}E_2$ chain

	ε/kJ mol^{-1}	σ/Å	q/e
C(1)	0.000 00	0.000	0.000
C(2)	0.478 12	3.983	0.290
O(3)	0.817 67	3.047	−0.580
C(4)	0.478 12	3.983	0.290
C(5)	0.478 12	3.983	0.290
O(6)	0.817 67	3.047	−0.580
C(7)	0.478 12	3.983	0.290
C(8)	0.478 12	3.983	0.290
O(9)	0.711 74	3.070	−0.700
H(10)	0.000 00	0.000	0.435

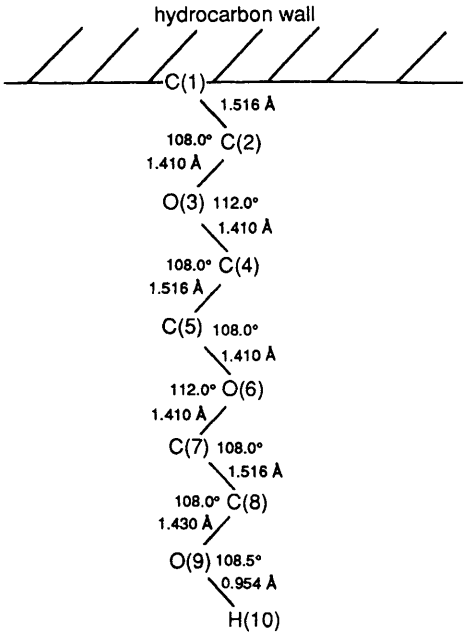

Fig. 3 OPLS geometry and atomic labels for the $C_{12}E_2$ chain

Table 2 OPLS torsional angle parameters for the $C_{12}E_2$ chain

chain bond	c_0/kJ mol^{-1}	c_1/kJ mol^{-1}	c_2/kJ mol^{-1}	c_3/kJ mol^{-1}
C(2)—O(3)	8.555 60	−3.502 20	5.853 00	17.910 80
O(3)—C(4)	8.555 60	−3.502 20	5.853 00	17.910 80
C(4)—C(5)	6.987 60	−17.747 50	0.887 60	25.622 80
C(5)—O(6)	8.555 60	−3.502 20	5.853 00	17.910 80
O(6)—C(7)	8.555 60	−3.502 20	5.853 00	17.910 80
C(7)—C(8)	6.987 60	−17.747 50	0.887 60	25.622 80
C(8)—O(9)	2.823 90	−2.945 40	0.485 70	6.255 00

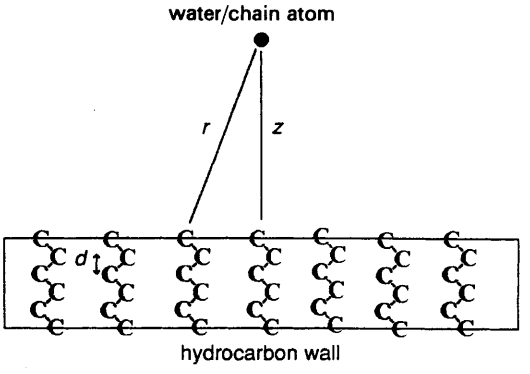

Fig. 4 Hydrocarbon wall consisting of an infinite number of layers of smeared out CH_2 united atoms

Table 3 OPLS wall parameters for the $C_{12}E_2$ hydrocarbon tails

	OPLS wall model
A_{ch}/Å^2	18.400[2]
d/Å	1.226 47
ε/kJ mol^{-1}	0.478 12
σ/Å	3.983

The wall–wall interaction was modelled as the interaction between slabs of smeared out CH_2 layers. The corresponding integrated potential is:

$$\frac{u}{A} \approx -\frac{\pi\varepsilon\sigma^6}{12A_{ch}^2 d^2 z^2} \quad (4)$$

Where d is the distance between the two bilayers.

Simulations of the $C_{12}E_2$ single chain in the canonical ensemble were performed at 298.15, 343.15, 353.15 and 363.15 K. For every 70 water-phase moves one chain rotation move was attempted. The probability of choosing any of the seven rotatable bonds was fixed and biased so that the free end of the chain is rotated more frequently. No terms for long-range corrections were included. The O—O, O—H and H—H radial distributions for water–water atoms were sampled together with the singlet distribution for oxygen in water with respect to the solid surfaces. Water oxygen–chain atom and hydrogen–chain atom radial distributions were also sampled together with the distribution of torsional angles along the surfactant chain.

Results and Discussion

The length of the simulations and the mean system energies per water molecule are given in Table 4. The chain torsional angles were sampled using the conformation labelling convention of *cis*, *gauche* and *trans* as shown in Fig. 5.

Table 4 Energies of the $C_{12}E_2$ single chain

T/K	phase moves /10^6	rotation moves /10^6	U/kJ mol^{-1} (per water)
298.15	92.80	1.33	−41.1841
343.15	104.30	1.49	−39.1508
353.15	133.05	1.90	−38.6415
363.15	131.75	1.88	−38.2624

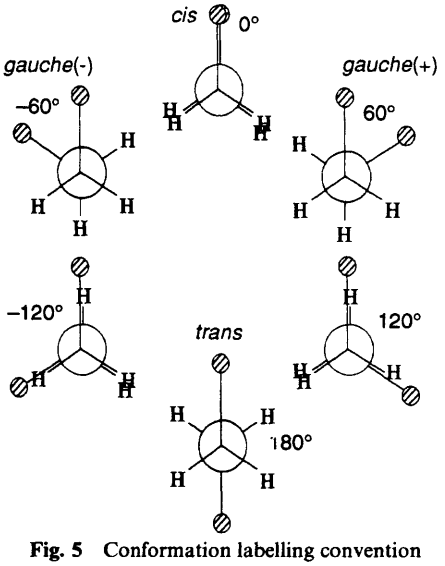

Fig. 5 Conformation labelling convention

At normal temperatures of 298.15 K the torsional angles about the C—O bonds were found to favour the *trans* conformation; whereas the C—C bonds prefer the *gauche* conformation (Fig. 6). When the temperature was increased the statistical sampling of the torsional conformations improved because of the more favourable energetics of chain conformational changes and both *gauche* configurations are observed (Fig. 7).

There was a strong tendency for water to form H-bond 'bridges' between oxygens on the chain at the lower temperatures (Fig. 8 and 9). This bridging mechanism requires the C—C bond to be in the *gauche* conformation and the adjacent C—O bond to be in the *trans* form. This conformation gives favourable H-bonding angles in the water–chain bridging complex as shown schematically in Fig. 10. As the temperature is raised the higher-energy *trans* conformations around the C—C bonds became more frequent and the chain can adopt conformations which are less linear. The chain appears to be adsorbed more strongly to the hydrocarbon wall and water bridging between the chain oxygens is less common. The snapshot in Fig. 11, taken from a run at 363.15 K, illustrates these points. This increase in adsorption of the chain onto the hydrocarbon wall suggests that the wall–chain interactions are now dominant. In addition the increased entropy in the system causes the water molecules in the vicinity of the chain to form less well defined hydrogen bonds, which weakens the water–chain interactions.

The water singlet distribution between the hydrophobic walls provides evidence that the water forms a layer structure

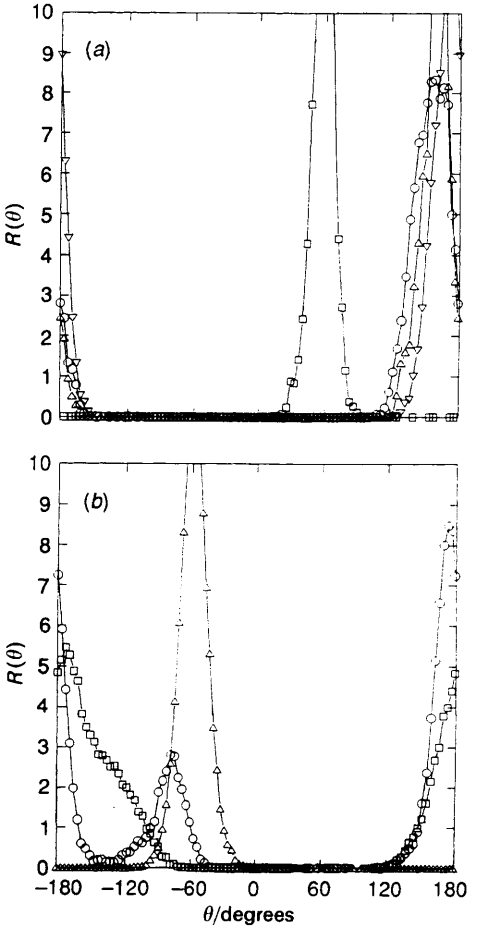

Fig. 6 Singlet angular distribution function of a $C_{12}E_2$ chain in SPC water at 298.15 K. (*a*) ○, C(2)—O(3); △, O(3)—C(4); □, C(4)—C(5); ▽, C(5)—C(6). (*b*) ○, O(6)—C(7); △, C(7)—C(8); □, C(8)—C(9).

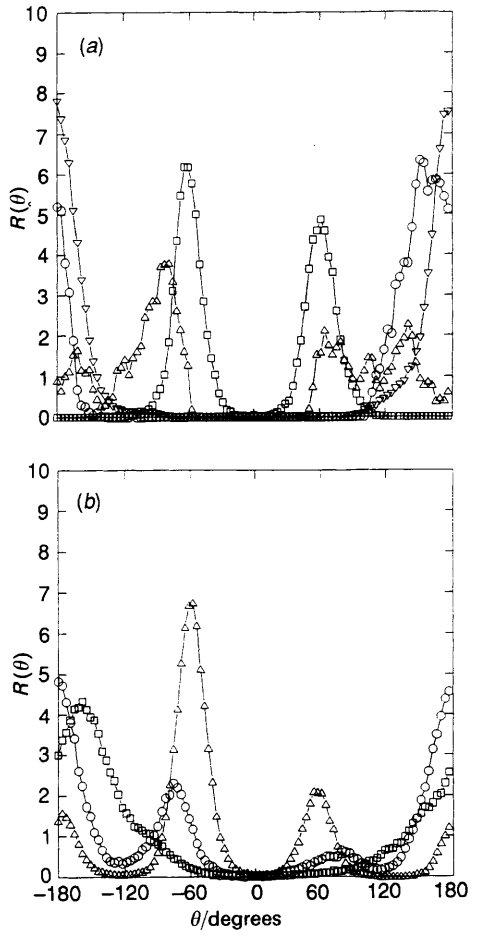

Fig. 7 Singlet angular distribution function of a $C_{12}E_2$ chain in SPC water at 363.15 K. (*a*) ○, C(2)—O(3); △, O(3)—C(4); □, C(4)—C(5); ▽, C(5)—C(6). (*b*) ○, O(6)—C(7); △, C(7)—C(8); □, C(8)—C(9).

between the walls. The water density was sampled in three separate *xy* zones as shown in Fig. 12. The first region, zone 0, is the region of the simulation box where the chain is fixed at $z = 0$ Å and zone 2 is the diagonally opposite region. The water distribution at 298.15 K (Fig. 13) has a strong peak at *ca.* 3.3 Å at both walls. This is caused by water layering

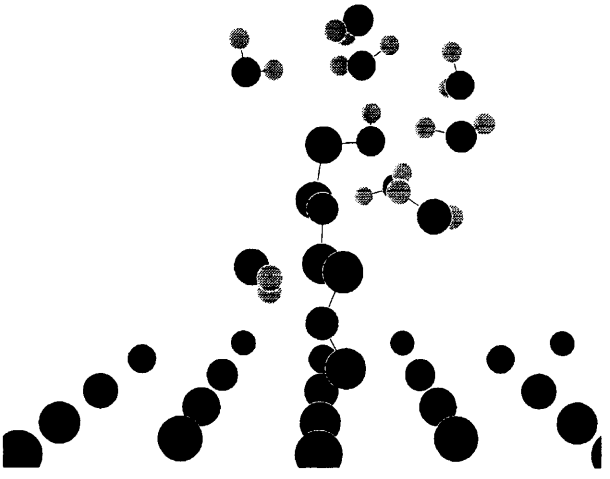

Fig. 8 Snapshot of a $C_{12}E_2$ chain in SPC water at 298.15 K after 20.30×10^6 water-phase and 0.29×10^6 chain-rotational trial moves. All water molecules at distances greater than 3.5 Å from the nearest chain atom have been removed from the picture.

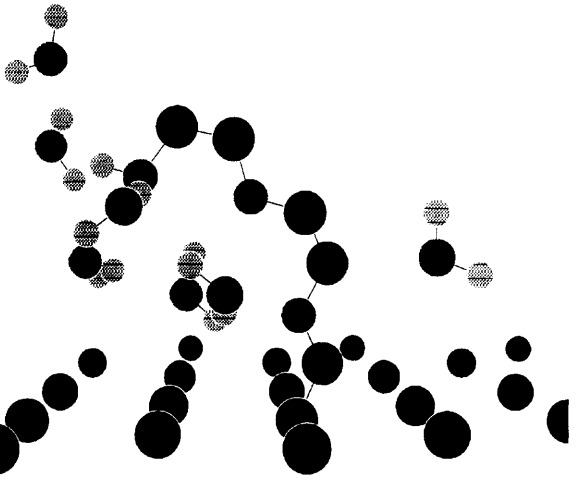

Fig. 9 As Fig. 8 after 56.75×10^6 water phase and 0.81×10^6 chain-rotational trial moves

at the surface of the wall. A secondary weaker peak appears at *ca.* 6 Å and in the central region the water density is approximately that of normal water. The zones 1 and 2 showed similar water distributions. However in zone 0, where the chain was attached, the water density in the region 3–7 Å has been reduced owing to the presence of the chain atoms. In the half of the box between 13 Å and 18 Å the three zones have almost identical water distribution because of the distance from the attached chain. Fig. 14 shows singlet water distributions at 363.15 K. The four peaks have now become broader as the water layers become less well defined. The intensity of the peaks in zone 0 at *ca.* 3.3 Å became weaker

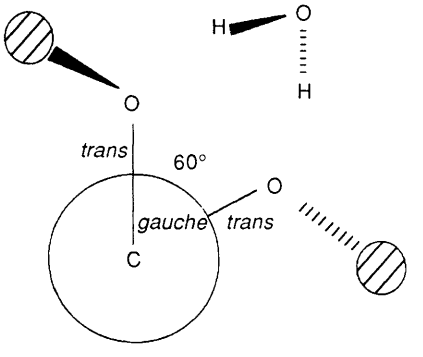

Fig. 10 Water H-bond bridging between chain oxygens

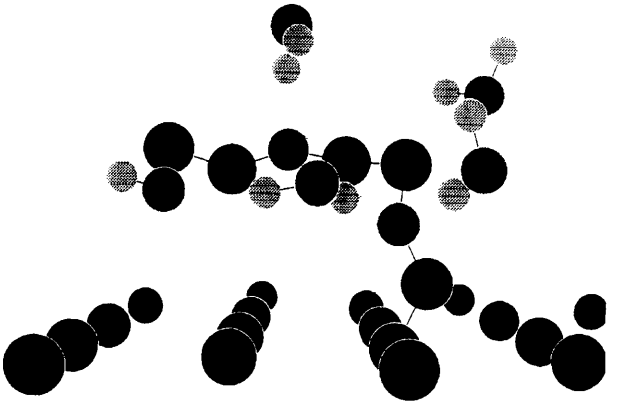

Fig. 11 As for Fig. 8 at 363.15 K after 131.75×10^6 water-phase and 1.88×10^6 chain-rotational trial moves

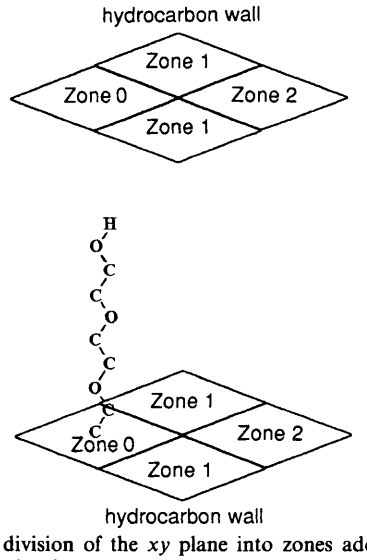

Fig. 12 The division of the *xy* plane into zones adopted in water singlet distribution functions

while the peak at 6 Å was stronger. This is evidence that at higher temperatures the chain preferred configurations which are closer to the wall, hence displacing the water into the central region.

Further information about the structure of water in the vicinity of the chain is given by the water–chain radial distribution functions shown in Fig. 15 for a temperature of 298.15 K. The general shapes of the distributions are recognisable from studies of bulk water. The expected nearest-neighbour separation for oxygen with oxygen is *ca.* 2.8 Å. Peaks at this distance appear with increasing strength as the chain oxygens O(3), O(6) and O(9) become more distant from the surface. At O(6) there is also a strong broad maximum centred around 5 Å which can be attributed to the water molecules which are hydrogen bonded to the neighbouring oxygens O(3) and O(9). The change in intensity of the first peak can be attributed to the presence of the wall which reduces the probability of finding a water molecule near to a given chain atom. The effect of water bound to adjacent oxygens is also seen in the O—H distributions, these show

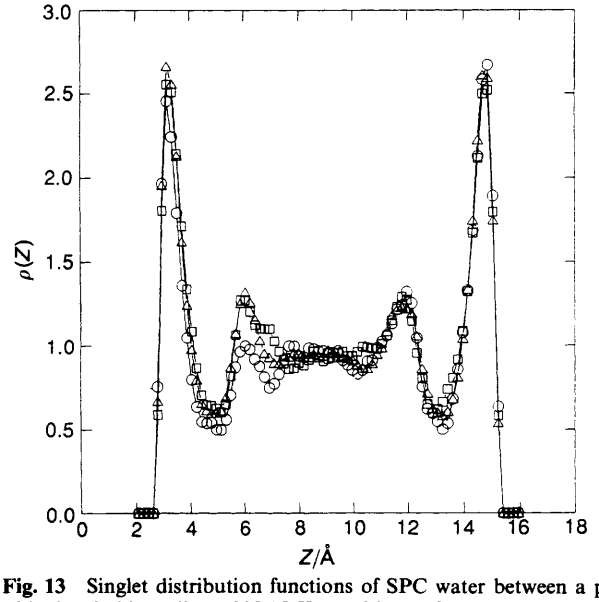

Fig. 13 Singlet distribution functions of SPC water between a pair of hydrophobic walls at 298.15 K. ○, Mean of zone 0; △, mean of zone 1; □, mean of zone 2.

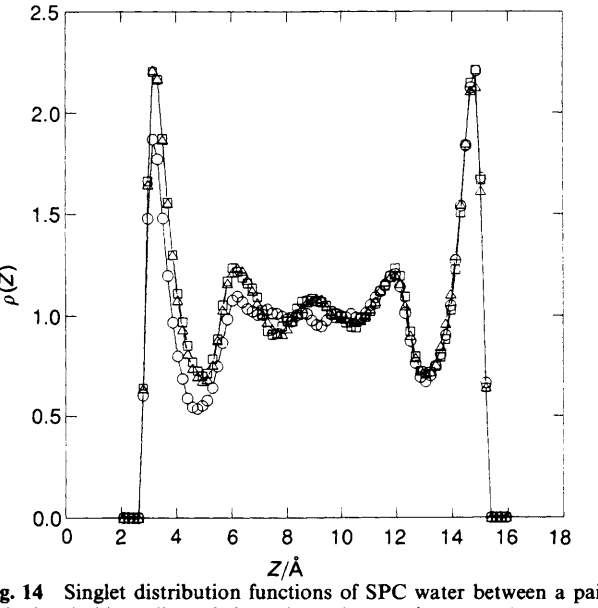

Fig. 14 Singlet distribution functions of SPC water between a pair of hydrophobic walls at 363.15 K. ○, Mean of zone 0; △, mean of zone 1; □, mean of zone 2.

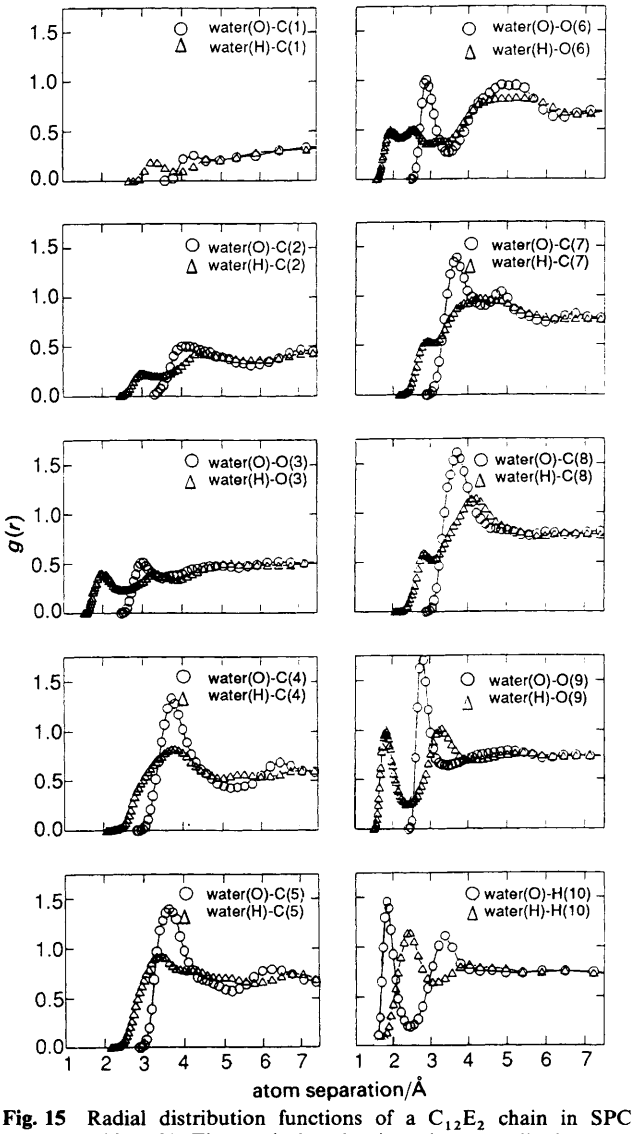

Fig. 15 Radial distribution functions of a $C_{12}E_2$ chain in SPC water at 298.15 K. The vertical scale gives the normalised water–chain $g(r)$ distributions and the horizontal scale is the atom separation in Å.

the characteristic H-bond first maximum at *ca.* 2 Å, but the second maximum is closer than in liquid water (*ca.* 3.2 Å *cf.* *ca.* 3.9 Å). This distance reflects the position of the second of the bridged oxygens. At the central of the three chain oxygens O(6) there is a more complex structure in the O—O distribution, because of a secondary peak at *ca.* 5 Å due to the water H bonding to O(3) and O(9).

The water distributions fall into three groups. At C(1) and C(2) the distributions are generally of low intensity, reflecting the fact that water is largely excluded from this region. In the central region at C(4) and C(5), the oxygen distributions are very similar with a well defined first-neighbour maximum at 3.8 Å and a weaker second maximum at *ca.* 6.2 Å. The broad C—H maximum also centres around this separation suggesting that the water tends to rotate freely rather than adopt localised structures near to these carbons. Similar trends can be observed near to C(7) and C(8), but here there is more evidence of structures with more intense oxygen peaks and some resolution of the maximum in the C—H distributions. The overall view which emerges is the contrast between the oxygen and CH_2 regions of the chain. The former tend to promote well defined structures.

Conclusion

The simulation of a single poly(oxyethylene) $C_{12}E_2$ chain headgroup fixed on a bilayer at a given bilayer separation has shown the tendency of water molecules to be well ordered around the chain headgroup.

Water–chain hydrogen bonding reveals a tendency to form water bridges between oxygens within the chain. The bridging mechanism requires conformations in which the C—C bonds are *gauche* and the C—O bonds *trans* to form complexes. At higher temperatures water bridging becomes weaker and the chain is adsorbed more strongly to the wall as a result of weaker water–chain interactions.

We are indebted to the SERC and Unilever Research for supporting this CASE project and for a generous allocation of computing time on the University of London C3860 Convex supercomputer.

References

1 M. Carvell, D. G. Hall, I. G. Lyle and G. J. T. Tiddy, *Faraday Discuss. Chem. Soc.*, 1986, **81**, 223.
2 I. G. Lyle and G. J. T. Tiddy, *Chem. Phys. Lett.*, 1986, **124**, 432.
3 P. M. Claesson, R. Kjellander, P. Stenius and H. K. Christenson, *J. Chem. Soc., Faraday Trans.*, 1986, **82**, 2735.
4 W. Helfrich, *Z. Naturforsch. A*, 1978, **33**, 305.
5 M. Grandfeldt, B. Jönsson and H. Wennerström, *Mol. Phys.*, 1988, **64**, 129.
6 B. Jönsson and H. Wennerström, *J. Chem. Soc., Faraday Trans.*, 1983, **79**, 19.
7 P. Attard and D. J. Mitchell, *J. Chem. Phys.*, 1988, **88**, 4391.
8 B. A. Bergenstahl and P. Stenius, *J. Phys. Chem.*, 1987, **91**, 5944.
9 S. Marčelja and N. Radic, *Chem. Phys. Lett.*, 1976, **42**, 129.
10 D. W. R. Gruen, S. Marčelja and B. A. Pailthorpe, *Chem. Phys. Lett.*, 1981, **82**, 315.
11 D. W. R. Gruen and S. Marčelja, *J. Chem. Soc., Faraday Trans.*, 1983, **79**, 211.
12 R. Kjellander and S. Marčelja, *Chem. Phys. Lett.*, 1986, **127**, 402.
13 R. F. Cracknell, PhD Thesis, University of London, 1990.
14 R. F. Cracknell, D. Nicholson and N. G. Parsonage, *Mol. Phys.*, 1992, **75**, 1023.
15 R. F. Cracknell, D. Nicholson and N. G. Parsonage, *Mol. Phys.*, 1992, **75**, 1039.
16 H. J. C. Berendsen, J. P. M. Postma, W. F. van Gunsteren and J. Herman, *Intermolecular Forces*, ed. B. Pullman, Reidel, Dordrecht, Holland, 1981, p. 331.
17 W. L. Jorgensen, *J. Phys. Chem.*, 1986, **90**, 1276.
18 W. L. Jorgensen and M. Ibraham, *J. Am. Chem. Soc.*, 1981, **103**, 3976.

Paper 4/00036F; *Received* 5*th January*, 1994